Early precipitation during cooling of an Al-Zn-Mg-Cu alloy revealed by *in situ* small angle X-ray scattering

P. Schloth,[1,2] J. N. Wagner,[3] J. L. Fife,[4] A. Menzel,[4] J.-M. Drezet,[1] and H. Van Swygenhoven[2,3]
[1]*Ecole Polytechnique Fédérale de Lausanne, Computational Materials Laboratory, Station 12, 1015 Lausanne, Switzerland*
[2]*Ecole Polytechnique Fédérale de Lausanne, Neutrons and X-rays for Mechanics of Materials, 1015 Lausanne, Switzerland*
[3]*Paul Scherrer Institut, Materials Science and Simulation, ASQ/NUM, 5232 Villigen-PSI, Switzerland*
[4]*Paul Scherrer Institut, Swiss Light Source, 5232 Villigen-PSI, Switzerland*

(Received 23 May 2014; accepted 25 August 2014; published online 12 September 2014)

Early subnanometre cluster formation during quenching of a high-strength AA7449 aluminium alloy was investigated using *in situ* small angle X-ray scattering. Fast quench cooling was obtained by using a laser-based heating system. The size and number density of homogeneous nucleated clusters were found to be strongly dependent on the cooling rate, while the volume fraction of cluster formation is independent of the cooling rate. Heterogeneous larger precipitation starts at higher temperatures in volume fractions that depend on the cooling rate. © *2014 AIP Publishing LLC*.
[http://dx.doi.org/10.1063/1.4894768]

The fabrication of aluminium alloys involves a number of thermomechanical steps such as solute-heat treatment followed by fast cooling, i.e., quenching. It is well known that the cooling rate influences the homogeneous and heterogeneous formation of precipitates and that the effect of these differences on the mechanical properties cannot be removed by additional aging. The typical precipitation sequence of the equilibrium η phase ($Mg(Zn,Cu,Al)_2$) in the Al-Zn-Mg(-Cu) system is: GPZ $\rightarrow \eta' \rightarrow \eta$.[1] Early studies by Lendvai and Löffler on Al-Zn-Mg alloys report that vacancy-rich clusters (VRC), acting as nucleation sites for Guinier Preston zones (GPZ), can form during the cooling from the solutionizing temperature.[2,3] The number of VRCs strongly depends on the quench parameters influencing the excess vacancies in the structure. Clusters formed by only a few atoms[4] have been identified using 3D atom probe. Despite their small size, the clusters are effective in increasing the yield strength of the material.[5] In addition to the VRCs, heterogeneous precipitation of the equilibrium η phase occurs at higher temperatures.[1] It is therefore not surprising that when producing thick Al alloy plates, the resultant precipitation size, density, and volume fraction are expected to differ across the plate because of the difference in cooling rates. The latter creates residual stresses at as quenched temper that are reduced by stress relief. The remaining residual stresses at final temper may lead to machining distortions. To investigate the influence of precipitation on residual stresses, thermomechanical models linking solid-state transformations to the final stress distribution have to be developed. Such simulation schemes need input on size, density, and volume fraction of precipitation as function of cooling rates that can only be provided by experimentation.

Small angle X-ray scattering (SAXS) has proven to be a useful tool for the investigation of precipitation phenomena.[6] SAXS is a well established technique for investigating clusters with high contrast in atomic number with respect to the matrix. SAXS has been used extensively to study precipitation phenomena in Al alloys ex situ and also *in situ* during aging.[6–8] Providing information on the size and volume fraction of the precipitates, SAXS validated thermodynamic-based precipitation model predictions[7,9] of the effect of aging on precipitation. There is however no information to be gathered available on precipitation during rapid cooling. The high brilliance of modern synchrotron sources allows information with a time resolution in the range of seconds and even nanoseconds.[10–14] In this work, we report on homogeneous and heterogenenous nucleation and growth of precipitates in an Al-Zn-Mg-Cu alloy during *in situ* rapid cooling in a SAXS environment.

A commercial high strength AA7449 alloy (Al-7.5–8.7 Zn-1.8–2.7 Mg-1.4–2.1 Cu wt. %) was used for this study. The specimens were taken from the quarter thickness of a 75 mm plate featuring a size of $3 \times 25 \times 0.5$ mm. The samples were solutionized for 1 h at 474 °C and quenched in water to dissolve residual precipitation. To minimize natural aging effects, the samples were stored in a freezer at—20 °C. The SAXS experiments were performed at the cSAXS beamline of the Swiss Light Source (SLS) at the Paul Scherrer Institut (PSI, Villigen Switzerland). The samples were positioned upright, and a laser-based heating system,[11] which was originally designed for the TOMCAT beamline of the SLS, was installed around the sample position. Homogeneous radial heat distribution was ensured in the sample by heating the sample from both sides at the same height. This setup allows the solution heat treatment and subsequent fast quenching of the sample by carefully controlling the power of the lasers. The temperature profiles were PID controlled by manipulating the output power of the lasers based on the temperature readings from a K-type thermocouple. The thermocouple was attached to the sample by spot welding and reinforced by a two-component glue. The height of the heating location was positioned at the height of the X-ray beam, which was around 2 mm above the thermocouple. The temperature gradient between the heating

position and the thermocouple position was measured for different temperatures and accounted for in the applied temperature profile and during further data analysis.

The small angle X-ray scattering experiments were performed at a wavelength of 0.774 Å (16 keV). The distance between the sample and the Pilatus 2M pixel detector was 2.1 m giving an accessible scattering vector range of $0.007\,\text{Å}^{-1} \leq q \leq 1\,\text{Å}^{-1}$ (Figure 1). The beam diaphragm was completely opened ($\sim 200 \times 200\,\mu m^2$) to ensure good grain and measurement statistics. In order to observe the dynamic processes during quenching, detector patterns were recorded every 0.5 s. Before the quench, the samples were heated to solutionizing temperature at 474 °C and held for 7 min to homogenise the microstructure. Figure 2(c) illustrates the three cooling conditions, differing in quench rates that were applied to cool the samples to room temperature. The slow and the medium quench (SQ and MQ, respectively) rates were realised by 3 linear temperature ramps. The fastest quench (FQ) rate was achieved by switching off the lasers. The FQ rate cooled the specimen from the solutionizing temperature to 200 °C in 10 s, corresponding to a cooling rate of about −25 K/s. The MQ and SQ curves incorporated slower cooling rates of about −15 K/s and −5 K/s between 420 and 200 °C and therefore required longer total cooling times (20 s and 45 s, respectively). At lower temperatures, the cooling rate is similar to Newtonian cooling. The time to reach near room temperature (35 °C) from 200 °C is 95 s, 180 s, and 245 s for the FQ, MQ, and SQ samples, respectively.

Inspection of the 2D SAXS distributions revealed isotropic scattering for all scattering angles, and thus, the intensity for each scattering vector was azimuthally averaged. In order to further increase the measurement statistics, the detector images taken during the quench from solutionizing to room temperature were averaged over 100 equidistant temperature segments ($\Delta T \approx 4.5$ K). The scattering spectra at the solutionizing temperature were used for background subtraction. The absolute intensity was calibrated using glassy carbon as a secondary standard.[15] Structural information, such as Guinier radius (R_g) and scattering invariant (Q), were extracted from the scattering data by using a model-independent analysis as performed by Deschamps and de

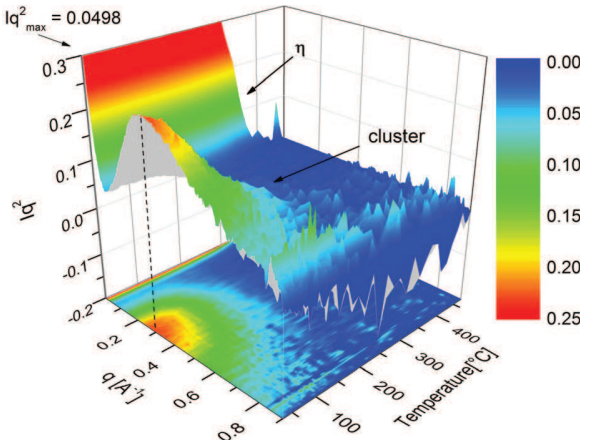

FIG. 1. The Kratky plot (Iq^2 vs q) as a function of temperature for the fastest quench (FQ). The Iq^2 scale in the Kratky plot was set to a value of 0.3 in order to better observe the evolution at high-q.

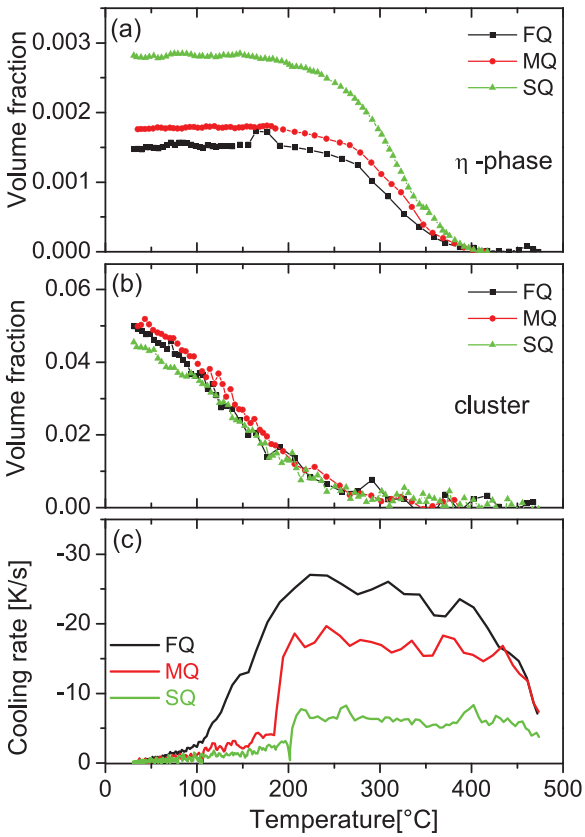

FIG. 2. Evolution of (a) the volume fraction of the η phase, (b) the volume fraction of clusters, and (c) the cooling rates of the three quenches as function of temperature.

Geuser.[16,17] The average particle size was estimated using a self-consistent Guinier approximation.[16] The uncertainty of the Guinier radius was calculated from the error associated with the slope of the linear Guinier fit. The volume fractions of the two phases were obtained from the scattering invariant, which corresponds to the integral of the Kratky plot from 0 to infinity.[17] The minimum between the two scattering contributions in the Kratky plot (Figure 1) was used to separate the invariants of both phases. The contribution at high q-values was extrapolated from a q-value of $0.07\,\text{Å}^{-1}$ to 0, instead of $0.007\,\text{Å}^{-1}$ for the whole scattering spectra. The contribution at low q-values was calculated as the difference of the two integrals. Assuming a two-phase model for the microstructure, the volume fraction, f_v, can be calculated from the scattering invariant as $Q = \int_0^\infty I(q)q^2dq = 2\pi^2(\Delta\rho)^2 f_v(1-f_v)$, where I is the absolute scattered intensity and $\Delta\rho$ is the difference in the scattering length density between the matrix and the precipitate. The scattering vector q was calculated as $q = 4\pi/\lambda \sin(2\theta/2)$, where λ is the wavelength and 2θ the scattering angle. The chemical composition of the precipitates was assumed to be 24.5 Al, 36 Zn, 34 Mg, 5.5 Cu for the clusters[18,19] and 14.6 Al, 38.3 Zn 33.3 Mg, 13.8 Cu for the η phase (in at %).[20] The accuracy of the volume fraction estimation cannot be expected to be better than ±10% due to the uncertainties related to the absolute intensity calibration, the extrapolations of the data in low-q and high-q regions, and assumptions of the chemical composition.[17] The number density of the precipitates

was calculated by $N = f_v/(4/3\pi R_g^3)$. It has to be noted that, due to the measurable momentum transfer having been limited to $q \geq 0.007\,\text{Å}^{-1}$, the Guinier radius could not be measured reliably for the η phase. This leads to an underestimation of the η volume fraction since part of the scattering contribution is cut off. Yet, the underestimated volume fraction still provides a good estimate of the temperature range of the η formation. Further, the reproducibility of the setup was verified by applying the same cooling conditions to two different samples for two different quench rates, which give similar results in both cases.

Figure 1 illustrates an example of the scattering dependence on applied temperature using the Kratky representation (Iq^2 vs q). Since the scattering curve at the solutionizing temperature was used for the background subtraction of the data, no scattering effects can be observed at the solutionizing temperature. During cooling, two scattering phenomena were observed and were seen regardless of the applied quench speed. First, upon cooling, for small q values, the intensity increases dramatically, which indicates large-scale scatterers (Figure 1). These objects refer to the equilibrium η phase, which is known to precipitate heterogeneously on dispersoids and grain boundaries. The volume fraction and size, typically ranging from 10 to 100 nm, depend strongly on the cooling rate. Heterogeneous precipitation at higher temperatures is undesirable since it lowers the mechanical properties such as yield strength, toughness, and fatigue in the resulting material.[1] It is evident that the cooling rate of -25 K/s is not fast enough to avoid heterogeneous precipitation at high temperatures in this alloy. Figure 2(a) illustrates the volume fraction evolution of η for the three cooling rates. In each sample, the scattering from η precipitates starts around 400 °C and saturates around 200 °C. Moreover, the formation of η clearly increases with decreasing cooling rate, which is expected due to longer time at high temperature.

Figure 1 also shows that further cooling leads to an increase in the scattering intensity around a q-value of $0.3\,\text{Å}^{-1}$. This indicates that the scatter is within a length scale of a nanometer, which corresponds to a cluster or GPZ. In addition, the observed isotropic scattering points to cluster/GP zones with a "blocky" and no 2D structure directly after quench, as was proposed in Ref. 18. The volume fraction of the small scatterers starts to increase at around 300 °C and increases as temperature decreases to room temperature (Figure 2(b)). This is a useful input for precipitation modeling since it describes the temperature range in which small clusters form during quench.

The cluster volume fraction evolution is similar for the three cooling rates, and no clear dependence on the cooling rate is observed. This is unexpected since faster quenching should lead to less precipitation. The slow quench features the lowest volume fraction of clusters (4.5%) compared to the fast and medium quenches, which both exhibit slightly higher volume fractions of clusters (4.9% and 5.0%, respectively) at the conclusion of quenching.

In contrast to the η phase, the cluster size is rather small. The Guinier radius is illustrated as function of temperature in Figure 3(a) together with the estimated error. A decreasing Guinier radius can be observed between 290 °C and 220 °C, which can be related to the decrease of the critical radius as

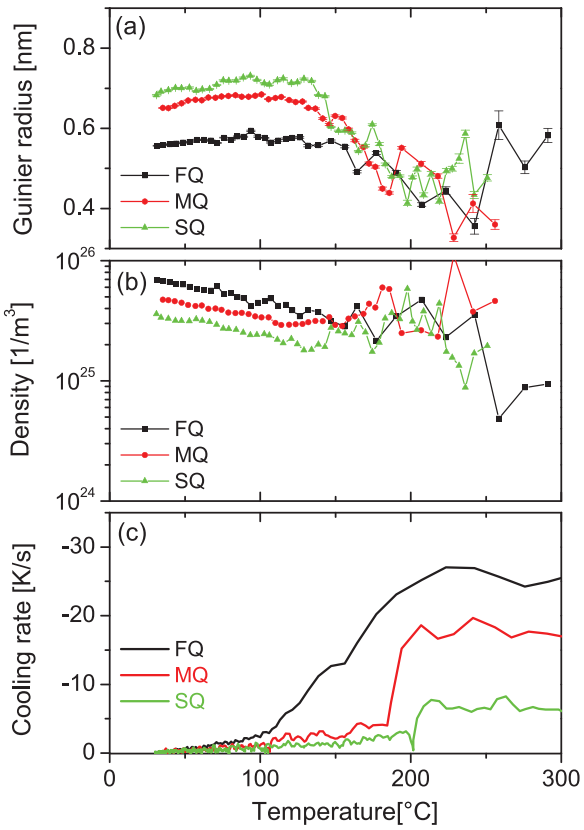

FIG. 3. Evolution of the Guinier radius (solid lines) and the number density (solid lines) of the clusters is shown together with the cooling rates (dashed lines) as a function of temperature for the three samples.

the temperature decreases. However, the scattering signal at high-q in this temperature region is low and the uncertainty of the Guinier radius is high. During further cooling to 100 °C, the Guinier radius of the clusters increases rapidly. The cluster growth depends clearly on the cooling conditions: the radius is largest (~0.72 nm) for the slow quench condition and smallest (~0.55 nm) for the fastest quench. Further cooling to room temperature shows a decrease in the average radius of the cluster. This indicates that limited mobility inhibits further growth of the existing clusters, but that ongoing nucleation of new clusters or GPZ with a smaller critical radius than the average size of the clusters already present in the sample does occur.

Figure 3(b) shows the calculated number density of clusters as a function of temperature. The cluster density, which is calculated from the Guinier radius and the volume fraction, increases continuously in all three cases. Yet, there are deviations from continuous growth between 220 °C and 150 °C, where the size estimation becomes difficult. This is particularly true around 150 °C, where the decrease in cluster density is not natural and indicates an underestimated cluster size; this in turn leads to an overestimation of the cluster density. Overall, the density of cluster is highest in the fast quench and lowest in the slowest quench sample. Slower cooling rates at higher temperatures lead to a lower density of excess vacancies at lower temperatures.[21] This could explain the lower number density of clusters for lower cooling rates since early clustering is strongly influenced by the number of excess vacancies, as reported by Lendvai[3] but not

yet seen in experimentation. It might also explain the same volume fraction evolution for the three cooling rates. The longer time for precipitation during slower quench speed is balanced by a smaller amount of excess vacancies due to their annihilation on defects. In addition to the vacancies that influence the clustering, the solute loss by the η precipitation can also influence the cluster formation by decreasing the thermodynamic driving force. The observed early clustering would have a marked effect on the yield strength of the material due to cluster strengthening. It would also have a pronounced influence on the residual stress build-up during quenching of large components.

In conclusion, *in situ* time-resolved SAXS measurements during quenching of an AA7449 aluminium alloy revealed the cooling rate dependence of homogeneous cluster formation. Subnanometre clustering starts around 300 °C. The average size of the clusters at room temperature depends strongly on the cooling rate, where larger cluster sizes occur at slower cooling rates. The cluster density increases with faster cooling rates, which can be ascribed to the higher number of excess vacancies when cooling speed is increased. Interestingly, the evolution of the volume fraction of clusters during cooling is very similar for all cooling rates. Finally, heterogeneous formation of precipitates during cooling takes place in the temperature regime between 400 and 200 °C and is more pronounced at lower cooling rates.

Our results bring new insights into homogeneous and heterogeneous nucleation and growth of precipitates, providing valuable input for simulations attempting to predict residual stresses in thick plates. We anticipate that the *in situ* experiment developed here can be optimized for cooling rates closer to those reached during additive manufacturing, and as such, will contribute to understanding the differences in microstructures and residual stresses among the various manufacturing methods. Future developments of high-intensity and ultra-fast scattering methods such as the free-electron laser will further enhance the value of *in situ* cooling experiments.

The research was funded by the Competence Center for Materials Science and Technology (CCMX, http://www.ccmx.ch/) involving EPF Lausanne, PSI Villigen, Univ. de Bretagne Sud Lorient, Constellium CRV, and ABB Turbocharger. J.L.F. also acknowledges CCMX for funding. We thank Constellium CRV for providing the material.

[1]D. Godard, P. Archambault, E. Aeby-Gautier, and G. Lapasset, Acta Mater. **50**, 2319 (2002).
[2]H. Löffler, I. Kovacs, and J. Lendvai, J. Mater. Sci. **18**, 2215 (1983).
[3]J. Lendvai, Mater. Sci. Forum **217–222**, 43–56 (1996).
[4]R. Marceau, G. Sha, R. Ferragut, A. Dupasquier, and S. Ringer, Acta Mater. **58**, 4923 (2010).
[5]M. J. Starink and S. C. Wang, Acta Mater. **57**, 2376 (2009).
[6]A. Deschamps, T. Bastow, F. de Geuser, A. Hill, and C. Hutchinson, Acta Mater. **59**, 2918 (2011).
[7]M. Nicolas and A. Deschamps, Acta Mater. **51**, 6077 (2003).
[8]M. Dumont, W. Lefebvre, B. Doisneau-Cottignies, and A. Deschamps, Acta Mater. **53**, 2881 (2005).
[9]M. Perez, M. Dumont, and D. Acevedo-Reyes, Acta Mater. **56**, 2119 (2008).
[10]L. Aagesen, J. Fife, E. Lauridsen, and P. Voorhees, Scr. Mater. **64**, 394 (2011).
[11]J. L. Fife, M. Rappaz, M. Pistone, T. Celcer, G. Mikuljan, and M. Stampanoni, J. Synchrotron Radiat. **19**, 352 (2012).
[12]R. Mokso, F. Marone, S. Irvine, M. Nyvlt, D. Schwyn, K. Mader, G. K. Taylor, H. G. Krapp, M. Skeren, and M. Stampanoni, J. Phys. D: Appl. Phys. **46**, 494004 (2013).
[13]B. Abécassis, F. Testard, O. Spalla, and P. Barboux, Nano Lett. **7**, 1723 (2007).
[14]S. Ibrahimkutty, P. Wagener, A. Menzel, A. Plech, and S. Barcikowski, Appl. Phys. Lett. **101**, 103104 (2012).
[15]F. Zhang, J. Ilavsky, G. G. Long, J. P. G. Quintana, A. J. Allen, and P. R. Jemian, Metall. Mater. Trans. A **41**, 1151 (2010).
[16]A. Deschamps and F. De Geuser, J. Appl. Crystallogr. **44**, 343 (2011).
[17]A. Deschamps and F. Geuser, Metall. Mater. Trans. A **44**, 77 (2012).
[18]G. Sha and A. Cerezo, Acta Mater. **52**, 4503 (2004).
[19]A. Deschamps, F. De Geuser, Z. Horita, S. Lee, and G. Renou, Acta Mater. **66**, 105 (2014).
[20]T. Marlaud, A. Deschamps, F. Bley, W. Lefebvre, and B. Baroux, Acta Mater. **58**, 248 (2010).
[21]F. Fischer, J. Svoboda, F. Appel, and E. Kozeschnik, Acta Mater. **59**, 3463 (2011).